the H_2 ligand and give an intermediate value for α in eq 2. Alternatively, eq 1 does not apply in this case because of tunneling of H atoms between sites of low symmetry. Work is still required to explain the disagreement between observed and calculated line widths of the H_2 resonance in the ^1H NMR spectrum.

Acknowledgment. This research was supported by grants to R.H.M. from the Natural Sciences and Engineering Research Council of Canada and from the donors of the Petroleum Research Fund, administered by the American Chemical Society, and by a loan of ruthenium and osmium chlorides from Johnson-Matthey Co. We thank A. Maynard and N. Plavac for assistance in collecting the T_1 data and Professor Robert Crabtree for providing preprints of his work.

Note Added in Proof. Dr. L. Field has suggested privately that $T_1^{(min)}$ for **1Fe** may be short due to a paramagnetic state contributing to the relaxation. However, $T_1^{(min)}$ values for the terminal hydride of **1Fe**, **1Ru**, and **20s** are similar (Table III), a fact that goes against this suggestion.

Optical Determination of Magnetization Behavior: A Study of Unstable Metallocenes by Magnetic Circular Dichroism

Robin G. Graham,[†,1a] Roger Grinter,*[,1a] and Robin N. Perutz*[,1b]

Contribution from the School of Chemical Sciences, University of East Anglia, Norwich NR4 7TJ, U.K., and Department of Chemistry, University of York, York Y01 5DD, U.K. *Received February 17, 1988*

Abstract: In this paper we report the first application of magnetic circular dichroism (MCD) to determine the magnetization curves for unstable, matrix-isolated molecules. Curves are obtained by recording the MCD signal at fixed wavelength as a function of B/T over the magnetic field range 0–8 T. For each compound, the curve is recorded at 1.8 K and at another temperature between 6 and 17 K. Magnetization curves are reported for three unstable matrix-isolated metallocenes Cp_2M (M = Mo, W, Re; Cp = η^5-C_5H_5) with spin and orbitally degenerate ground states. They are compared to curves for matrix-isolated (η^5-C_5Me_5)$_2$Re reported earlier and for (tol)$_2$V (tol = η^6-toluene), which has a $^2A_1$ ground state. The data are analyzed by two methods. The first uses published methods for a random array of linear molecules. Assuming $g_\perp = 0$, values of $g_\parallel$ of 2.75 ± 0.18, 3.07 ± 0.15, and 5.34 ± 0.36 are determined for Cp_2M (M = Mo, W, and Re, respectively). The $g_\parallel$ value for Cp^*_2Re ($Cp^* = \eta^5$-C_5Me_5) and the isotropic g value for (η^6-tol)$_2$V (5.07 ± 0.19 and 1.94 ± 0.03, respectively) are in excellent agreement with determinations by EPR. In the second method of analysis, a quantum mechanical model including the effects of covalency, spin–orbit coupling, and low-symmetry distortion is used. The differential absorbance is evaluated for particular transitions as a function of B and T. A least-squares fitting procedure is then employed to determine the g values, the orbital reduction factor, and the distortion parameter at an assumed value of the spin–orbit coupling constant. The values of $g_\parallel$ determined by this method are in excellent agreement with the first method. This method also gives estimates of $g_\perp$, which prove to be as low as 0.05. These experiments demonstrate the power of optical determination of magnetization curves and g values for unstable molecules, some of which are EPR silent.

The measurement of the magnetization curve or the magnetic parameters of an unstable molecule presents many difficulties. The traditional response to this question is to use electron paramagnetic resonance, a method that has had spectacular success in many instances. However, there are drawbacks to EPR: (i) its high sensitivity compared to those of other spectroscopic methods renders it difficult to demonstrate that an EPR spectrum belongs to the same molecule as an absorption spectrum; (ii) more seriously, some molecules are EPR silent, although they are paramagnetic. EPR silence is encountered most frequently with molecules containing heavy elements and an even number of unpaired electrons. In such situations, zero-field splittings often exceed the operating frequency of the EPR spectrometer. There is also a group of molecules with orbital and spin angular momentum, which are EPR silent at room temperature, because they relax very rapidly, but which often become EPR detectable at very low temperature.[2]

We faced a combination of all these problems in studying the unstable metallocenes of tungsten, molybdenum, and rhenium, which we had generated by photolysis of the corresponding hydrides, Cp_2MH_n, and/or related Cp_2ML molecules (Cp = η^5-C_5H_5) in low-temperature matrices.[3,4] We turned instead to a quite different technique, magnetic circular dichroism (MCD).[5,6] Since the MCD spectra of these molecules exhibited the same intense, structured bands as the absorption spectra, we knew at once that we were studying the same molecules in MCD and in absorption. Moreover, the MCD signals increased in intensity as the temperature was lowered. This phenomenon, known as a C-term to MCD spectroscopists, is a sure indicator of paramagnetism. It arises from the increasing Boltzmann population of the lowest Zeeman state as the temperature is lowered or the magnetic flux density, B, is increased (Figure 1). We could take the analysis a stage further by examining the ratio of the integrated differential absorption to the integrated absorption (C/D).[5] When considered in conjunction with an analysis of the electronic states available to the metallocenes, this ratio gave an estimate of the value of $g_\parallel$. This approach proved beyond doubt that each of these molecules had high orbital angular momentum in the ground state, arising from the presence of a vacancy in the e_2 orbital (Figure 2).[6] Nevertheless, the use of band areas suffered from a number

[†] Current address: Department of Physics and Astronomy, University of St. Andrews, St. Andrews KY16 9SS, Scotland.

(1) (a) University of East Anglia. (b) University of York.

(2) E.g., see: Wertz, J. E.; Bolton, J. R. *Electron Spin Resonance, Elementary Theory and Practical Applications*; McGraw-Hill: New York, 1972.

(3) Chetwynd-Talbot, J.; Grebenik, P.; Perutz, R. N. *Inorg. Chem.* **1982**, *21*, 3647.

(4) Chetwynd-Talbot, J.; Grebenik, P.; Perutz, R. N.; Powell, M. H. A. *Inorg. Chem.* **1983**, *22*, 1675.

(5) Piepho, S. B.; Schatz, P. N. *Group Theory in Spectroscopy with Applications to Magnetic Circular Dichroism*; Wiley: New York, 1983.

(6) Cox, P. A.; Grebenik, P.; Perutz, R. N.; Robinson, M. D.; Grinter, R.; Stern, D. R. *Inorg. chem.* **1983**, *22*, 3614. Cox, P. A.; Grebenik, P.; Perutz, R. N.; Graham, R. G.; Grinter, R. *Chem. Phys. Lett.* **1984**, *108*, 415.

0002-7863/88/1510-7036$01.50/0

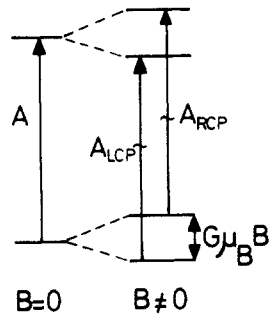

Figure 1. Schematic diagram showing the relationship between absorption and MCD. The ground term is split by $G\mu_B B$ where $G = Ng$ and N is the number of unpaired electrons. The selection rules permit absorption of left circularly polarized (LCP) light from one component and RCP light from the other.

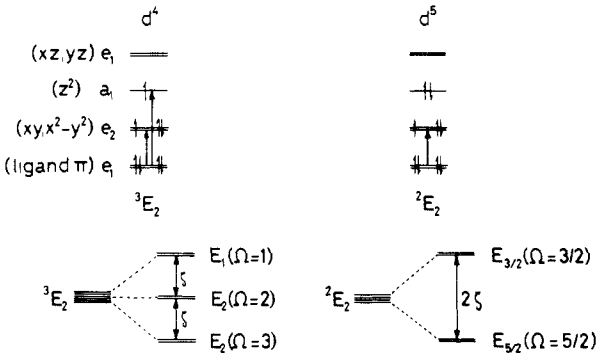

Figure 2. Above: Ground electron configurations and terms for d^4 and d^5 metallocenes showing the d orbitals and the highest occupied ligand orbitals. The arrows show the LMCT transitions under study. Below: Effect of spin–orbit coupling on the ground terms. The values of Ω refer to the total angular momentum quantum number.

of inaccuracies: we had to measure areas on the same sample with two different spectrometers, the short-wavelength limit for the band appeared to be different in the MCD and the absorption spectra, and we had to make arbitrary decisions about the base line in absorption, sometimes correcting for interference effects.

The theoretical work by Schatz, Mowery, and Krausz (SMK) demonstrated that there is an alternative approach to extracting ground-state magnetic parameters from MCD measurements.[7] If the temperature used is sufficiently low and the magnetic field sufficiently high, it should be possible to obtain a full magnetization curve by plotting the MCD intensity against B/T. Our first attempt at measuring a magnetization curve for Cp_2Re, described in a preliminary communication,[6] was qualitatively successful but showed the need for more accurate temperature and field measurement, and a lower limiting temperature. In conjunction with Oxford Instruments, R.G.G. and R.G. constructed a new matrix-isolation-MCD cryostat, which can reach 1.5 K and incorporates a superconducting magnet which can achieve 10 T.[8] The instrument is designed for optimal thermal contact between the matrix and the refrigerant and for very accurate measurement of B and T. Measurements are made by setting the dichrograph to a fixed wavelength, usually on a maximum in ΔA. The values of ΔA and B are then recorded as the magnetic field is ramped up from zero. The temperature is also measured for each of the ~300 points of the magnetization curve, although it varies only slightly during the measurement process.

We have already published a detailed description of the instrument and tests on a matrix-isolated molecule with a high-spin $^6A_1$ ground state, tris(acetylacetonato)iron(III).[8] We have also demonstrated its use as a part of a wider study of the open-shell decamethylmetallocene, Cp^*_2Re ($Cp^* = \eta^5$-C_5Me_5).[9] In this case we were able to compare valulue of $g_\parallel$ obtained by MCD magnetization in an argon matrix ($g_\parallel = 5.07 \pm 0.19$) with those obtained by EPR in frozen toluene ($g_\parallel = 5.081 \pm 0.003$). The excellent agreement demonstrated that the method could also be applied to molecules with high orbital angular momentum. We now report detailed MCD–magnetization studies of Cp_2M (M = Mo, W, Re). We analyze the results for these molecules and for Cp^*_2Re using both the SMK method and more detailed quantum mechanical models. We believe that these are the first optical determinations of magnetization and the magnetic parameters of unstable molecules using the MCD–magnetization method.

The metallocenes are of particular interest because their reactivity is very sensitive to electronic and steric effects. Metallocenes are stable for the first-row elements for all electron configurations from d^3 (15 electrons) to d^8 (20 electrons). Isolable metallocenes of second- and third-row transition metals are known only for the d^6 (18-electron) configuration, the only exception being the marginally stable rhodocene. Metallocenes of 16 and 17 electrons such as Cp_2M (M = Mo, W, Re) appear to be highly unstable with respect to dimerization and C–H bond activation processes and are known only when stabilized in an inert matrix[3,4,6] or as transient reaction intermediates.[10] The dimerization can be suppressed by permethylation, as is clear from the stability of Cp^*_2Re in the crystalline state. However, both Cp^*_2Re and Cp^*_2W appear to be unstable with respect to intramolecular C–H bond activation.[11]

The electronic structure of all the metallocenes is excellently described by a ligand field model.[9,12] In the LF model the d orbitals split into e_2 (xy, x^2-y^2), a_1 (z^2), and e_1 (xz, yz), in order of decreasing binding energy. Since the effect of conformation on their spectroscopic properties is almost negligible, we use symbols appropriate to D_5 symmetry. The highest occupied of the ligand orbitals has e_1 symmetry. It is from this orbital that the ligand-to-metal charge-transfer (LMCT) bands arise, which dominate the visible absorption spectra of 16- and 17-electron metallocenes. The electron configurations and the ground-state terms that arise from them are illustrated in Figure 2. They are also subject to spin–orbit coupling and low-symmetry Jahn–Teller (JT) distortions. In the third-row metallocenes, the spin–orbit effects are so large that they quench the JT distortion.[3,4,6] In the limit of zero distortion the g values are anticipated to be as follows:

$$d^4 \quad g_\parallel = 2(1 + k) \qquad g_\perp = 0$$

$$d^5 \quad g_\parallel = 2(1 + 2k) \qquad g_\perp = 0$$

where k is the orbital reduction factor.[12] However, it should be remembered that there are two unpaired electrons in the ground-state d^4 configuration, so the Zeeman splitting is $2g_\parallel$ or $8\mu_B B$ in the ionic ($k = 1$) limit. For the d^5 configuration, $g_\parallel$ reaches the value of 6 in the ionic, zero-distortion limit.

It is sometimes helpful to replace the D_5 group by the $C_{\infty v}$ point group, a method used especially by Warren.[12] The major correspondences are A_1:Σ, E_1:Π, E_2:Δ. The analogy is particularly helpful in pointing out that these three terms carry 0–2 units of orbital angular momentum, respectively. However, we discovered in the course of our previous analysis of MCD spectra of metallocenes that the transformation to the linear point group fails to show how the raising and lowering operators interconvert the states.[6] It also becomes unsuitable, when it is necessary to include low-symmetry distortions, so this method should be applied with care.

(7) Schatz, P. N.; Mowery, R. L.; Krausz, E. R. *Mol. Phys.* **1978**, *35*, 1537.
(8) Graham, R. G.; Grinter, R.; Stern, D. R.; Timms, K. *J. Phys. E.* **1986**, *19*, 776.
(9) Bandy, J. A.; Cloke, F. G. N.; Cooper, G.; Day, J. P.; Edelstein, N. M.; Graham, R. G.; Girling, R. N.; Green, J. C.; Grinter, R.; Perutz, R. N. *J. Am. Chem. Soc.* **1988**, *110*, 5039. Unfortunately, an earlier, incorrect value of $g_\parallel = 4.87$ for Cp^*_2Re appears in the abstract and the EPR section of this paper. The correct MCD value (Method I) is 5.07 as given here.
(10) Perutz, R. N.; Scaiano, J. C. *J. Chem. Soc., Chem. Commun.* **1984**, 457.
(11) Cloke, F. G. N.; Green, J. C.; Green, M. L. H.; Morley, C. P. *J. Chem. Soc., Chem. Commun.* **1985**, 945. Cloke, F. G. N., personal communication.
(12) Warren, K. D. *Struct. Bonding (Berlin)* **1976**, *27*, 45.

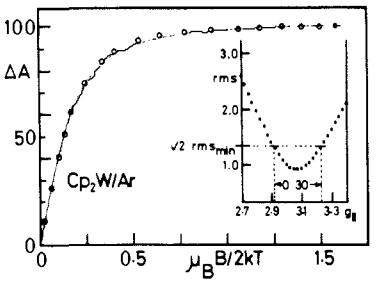

Figure 3. Magnetization curves for Cp_2W in an argon matrix. The small dots are the experimental points determined on the band maximum at 390 nm. The points measured at 1.8 K extend to higher values of $\mu_B B/2kT$. The points measured at 15 K reach to ca. 0.2 $\mu_B B/2kT$. The open circles show the points calculated by method II with the following parameter values: $k = 0.8$, $\delta = 1325$ cm^{-1} (see Table I). The inset shows the determination of $g_\parallel$ by method I. The root-mean-square deviation of ΔA(calcd) − ΔA(exptl) is plotted against $g_\parallel$. The error bars on $g_\parallel$ are obtained from the values predicted where the rms deviation is $\sqrt{2}$ times its minimum value.

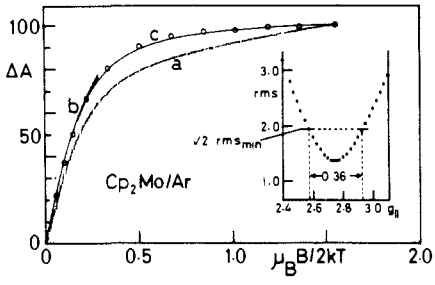

Figure 4. Magnetization curves for Cp_2Mo in an argon matrix. (a) Experimental curve at 1.8 K with data at 377 and 411.5 nm superimposed. (b) Experimental curve at 9.7 K with data from both wavelengths as in (a). (c) Curve obtained by correcting data obtained at 1.8 K for B-term; see text. The open circles show the calculated points using method II with the following parameter values $k = 0.6$, $\delta = 450$ cm^{-1} (see Table I). The inset shows the determination of $g_\parallel$ using method I; see Figure 3.

Experimental Section

The cryostat used for the MCD-matrix isolation studies is described in detail elsewhere.[8] The details of preparing the compounds and depositing the matrices are also reported in previous papers.[3,4,6]

Results and Analysis

1. Determination of the Magnetization Curves. Cp_2W and Cp_2Mo were prepared by photolysis of the corresponding dihydrides in Ar matrices at ca. 16 K. They both exhibit intense absorption and MCD bands close to 400 nm, which we have illustrated in a previous paper.[6] We have now determined magnetization curves for both molecules (Figures 3 and 4) at two different temperatures. In each case the curve is measured with the dichrograph set on one of the most intense maxima of the vibrational progression. The curve for WCp_2 measured at 15 K proves to be essentially superimposable on the one measured at 1.8 K. At 15 K the magnetization just begins to saturate at the highest field, but the curve recorded at 1.8 K shows complete saturation ($d(\Delta A)/dB = 0$) at 7–8 T. In the case of Cp_2Mo, we have measured the curves at two wavelengths and find that the curves are superimposable. However, the curves measured at different temperatures do not superimpose but nest inside one another. Moreover, at the lowest temperature, we find that the magnetization tends toward a straight line at high field but does not saturate. The origin of this phenomenon is discussed further below.

Rhenocene, Cp_2Re, was generated by photolysis of Cp_2ReH in nitrogen matrices. (It is not formed in Ar matrices, probably because of in-cage recombination.[4]) Its spectra (Figure 5) and magnetization curves (Figure 6) are qualitatively similar to those of the other metallocenes. Its magnetization curves measured at two temperatures are superimposable like those of Cp_2W, but it does not saturate as completely in the high-field limit.[2] The spectra

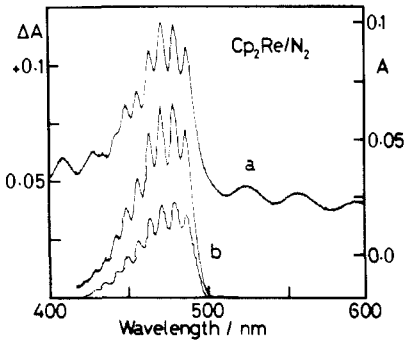

Figure 5. (a) Absorption spectrum of Cp_2Re in N_2 obtained by photolysis of matrix-isolated Cp_2ReH. The periodic structure in the base line is an interference pattern. (b) MCD spectra of the same matrix at 6 T and 16.5 K (broken line) and 1.8 K (continuous line).

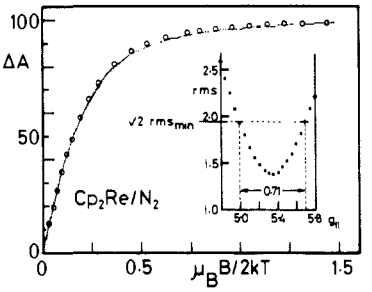

Figure 6. Magnetization curves for Cp_2Re in an N_2 matrix. The figure follows the same pattern as Figure 3. The experimental points were determined at 478 nm at temperatures of 1.8 and 6.5 K.

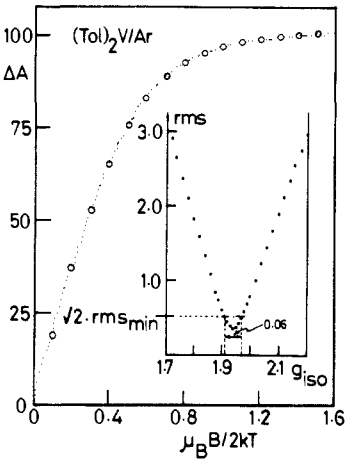

Figure 7. Magnetization curves for $(tol)_2V$ in an argon matrix. The figure follows the same pattern as Figure 3. The experimental points were determined at 445 nm at temperatures of 1.8 and 6.1 K.

and magnetization curves of Cp^*_2Re, illustrated in the paper on that complex, are very similar to those of Cp_2W and Cp_2Re.

For comparison we also recorded the spectrum and magnetization curve of a bis(arene)metal complex, $(tol)_2V$ (tol = η^6-toluene),[13] which has a $^2A_1$ ground state, well-known g values, and no orbital angular momentum. The magnetization curve was determined at 445 nm and is shown in Figure 7. The onset of curvature is seen to occur at a much higher value of $\mu_B B/2kT$ than in any of the other materials. This qualitative observation already indicates a lower g value for $(tol)_2V$. The curves at 1.8 and 6.1 K are almost superimposed, but full saturation is barely reached, even at 8 T.

2. Analysis of the Magnetization Curves. The MCD–magnetization/saturation phenomenon has been discussed in detail

(13) Cloke, F. G. N.; Dix, A. N.; Green, J. C.; Perutz, R. N., Seddon, C. J. *Organometallics* **1983**, *2*, 1150.
(14) Prins, R. *Mol. Phys.* **1970**, *19*, 603.

Table I. Molecular Parameters and g Values Obtained by Fitting the Magnetization Data

			simple axial model[a]		quantum mechanical ground-state models described in detail in text[b,c]					
	n[d]	λ[e]/nm	$g_\parallel$	rms[f]	k	ζ/cm^{-1}	δ/cm^{-1}	$g_\parallel$	$g_\perp$	rms[f]
Cp_2Mo[g]	26	411.5 and 377.0	2.75 ± 0.18	1.37	1.0	600[h]	1500	2.74	0.04	1.39
					0.8	600	900	2.75	0.04	1.38
					0.6	600	450	2.75	0.03	1.38
					0.4	600	90	2.75	0.01	1.38
					0.2	600	0	2.40	0.00	3.17
Cp_2W	30	390.0	3.07 ± 0.15	0.93	1.0	1500[i]	2350	3.08	0.01	0.91
					0.8	1500	1325	3.07	0.01	0.91
					0.6	1500	475	3.06	0.01	0.92
					0.4	1500	0	2.80	0.00	1.97
					0.2	1500	0	2.40	0.00	4.85
Cp_2Re	26	478.0	5.34 ± 0.36	1.38	0.825	1800[j]	0	5.30	0.00	1.39
Cp^*_2Re[k]	28	588.0	5.07[j] ± 0.19	0.60	0.77	1800[j]	0	5.08	0.00	0.62
$(tol)_2V$[l]	39	445.0	1.94[m] ± 0.03	0.36						

[a] Reference 7. [b] Reference 17. [c] Reference 15. [d] n = number of representative points selected from the original data. [e] Wavelength at which magnetization curve was measured. [f] rms = root-mean-square deviation = $[r^2/(n-2)]^{1/2}$. [g] For $MoCp_2$ the 1.8 and 10 K data were not superimposable. They could be superimposed by subtracting a B-term contribution from each, and this was done before fitting; see text. [h] Reference 21. [i] Reference 6. [j] Reference 9. [k] Decamethylrhenocene. [l] Bis(η^6-toluene)vanadium. [m] This molecule has spin angular momentum only, and the fit is to g_{iso} not $g_\parallel$.[20]

by Schatz, Mowery, and Krausz (SMK)[7] for the case of molecules belonging to $D_{\infty h}$ and its subgroups. For the analysis of the present data, the most useful starting point is provided by their eq 9–11, which we repeat here as eq 1–3 for the convenience of the reader.

$$\Delta\epsilon_0 = \frac{K}{Q_e'}\sum_{A'}\Delta a \exp(-E_{A'}/kT) \ldots \quad (1)$$

$$\Delta a = \sum_J [\cos\theta\{|\langle A'|m_-|J\rangle|^2 - |\langle A'|m_+|J\rangle|^2\} + \sqrt{2}\mathrm{Re}\sin\theta \exp(i\phi)\{\langle A'|m_+|J\rangle\langle A'|m_z|J\rangle^* - \langle A'|m_z|J\rangle\langle A'|m_-|J\rangle^*\}] \ldots \quad (2)$$

$$\langle\Delta\epsilon\rangle_0 = (1/8\pi^2)\int_0^{2\pi}\int_0^{2\pi}\int_0^{\pi}\Delta\epsilon_0 \sin\theta\, d\theta\, d\psi\, d\phi \ldots \quad (3)$$

Equation 1 expresses the zeroth moment of the MCD, $\Delta\epsilon_0$, in terms of the populations of the electronic components of the ground state A′, the partition coefficient, Q_e', and a collection of physical constants, K. Δa is defined by eq 2, which gives the magnetic field induced differential absorption of left and right circularly polarized light in terms of the matrix elements of the molecule-fixed transition dipole moment operator, m, between the ground state A′ and an excited state J. (The sums over A′ and J in eq 1 and 2 are over all electronic components of those states.) The Euler angles θ, ϕ, and ψ arise in the conversion from space-fixed to molecule-fixed axes. The operator Re takes the real part of everything to its right. Finally, in the case of randomly orientated molecules, we require to average $\Delta\epsilon_0$ over all possible orientations, a process expressed by eq 3. We may apply these equations to the analysis of our data in two ways.

2.1. Method I. In the first instance, we may follow SMK further and, assuming that $g_\perp = 0$, as it should for the metallocenes we are considering,[7] use eq 4 (their eq 12). Here $n =$

$$\langle\Delta\epsilon\rangle_0 = K'\int_0^1 n \tanh(nG_\parallel\mu_B B/2kT)\, dn \ldots \quad (4)$$

$\cos\theta$ and $K' = K\bar{m}^2$ with $\bar{m}_+ \equiv \langle i|m_+|f\rangle$, where $\langle i|$ and $|f\rangle$ are the initial and final states involved in the transition. $G_\parallel = Ng_\parallel$, where N is the number of unpaired electrons. The other parameters not previously defined have their usual meanings. A least-squares fit of eq 4 to our experimental data gives a value of $G_\parallel$. We extracted a series of representative values from the 200–300 experimental points and varied K' and $G_\parallel$ in eq 4 until a minimum in the root-mean-square deviation between the fitted and the experimental data was obtained. The integration over $\cos\theta$ was performed numerically with 10-point Gauss–Legendre quadrature. The insets in Figures 3, 4, and 6 illustrate the behavior of the deviation with variation of $g_\parallel$. The values of $g_\parallel$ obtained are listed in the left-hand portion of Table I. The errors listed in the table are obtained by examining the values of $g_\parallel$ at $\sqrt{2}$ times the minimum deviation. Although this figure is not chosen with a statistical basis, it is effective for comparing the quality of fit.

In the case of $(tol)_2V$, a system with spin angular momentum only, the g values are known to be almost isotropic ($g_\parallel = 2.00$, $g_\perp = 1.98$).[13] The magnetization curve is therefore expected to follow the function $\tanh(g_{iso}\mu_B B/2kT)$.[5] Figure 7 shows that the experimental data fit a simple tanh function. The best agreement is found with $g_{iso} = 1.94$.

As indicated above, the magnetization curves obtained at different temperatures superimpose on one another except in the case of Cp_2Mo, which shows "nesting". This nesting phenomenon and its possible origins will be discussed in more detail later in the paper; at this juncture we note that such behavior is incompatible with the assumptions underlying the derivation of eq 4. However, the long linear portion of the 1.7 K magnetization curve of Cp_2Mo (Figure 4) strongly suggests that the reason for the nesting is the mixing of electronic states by the magnetic field (B-terms). This effect was estimated from the slope of the 1.7 K magnetization curve at high field. Explicitly, the increase of ΔA with $\mu_B B/2kT$ above $\sim$1.25 was assumed to be entirely due to the B-term. When the B-term determined in this way is subtracted from the 1.7 and 9.7 K data, the two resulting curves are found to superimpose well. The B-term corrected and renormalized 1.7 K curve forms the data to which eq 4 (and other theoretical analyses) have been fitted for Cp_2Mo (Figure 4c).

The fact that EPR measurements on metallocenes have frequently revealed a $g_\parallel$ value[12] implies that $g_\perp \neq 0$[12,14] and that the molecule is probably not axial. This is because the value of $g_\perp$ and the probability of the $g_\parallel$ EPR transition both depend upon the matrix element of S_x (or S_y) between the components of the lowest doublet, which is zero for an axial geometry. In view of this result, we have used SMK's eq 17 to investigate whether the assumption of a nonzero $g_\perp$ value would improve the fit of our theoretical magnetization curves to the experimental data. In view of the excellent fits determined from eq 4, it is perhaps not surprising that no significant improvement was found.

2.2. Method II. Because of the generality of the SMK analysis, $g_\parallel$ emerges as an adjustable parameter. In order to obtain more detailed information concerning the features of the electronic structure that determine g, it is necessary to construct more specific quantum mechanical models of the systems under consideration. We now describe models for the d^4 and the d^5 molecules, in which two possible mechanisms are incorporated for the reduction of $g_\parallel$ from its limiting value. These mechanisms are covalent delocalization of the metal d electrons, parameterized by the orbital reduction factor k, and the quenching of the orbital angular momentum by a low-symmetry perturbation, δ, which also provides an explicit mechanism for the departure of $g_\perp$ from zero.

Our interpretation of the magnetization curves for the d^4 systems (Cp_2Mo and Cp_2W) is based upon a model for the ground state proposed by Krieger and Voitländer.[15] The d^5 data (Cp_2Re

Chart I

	$E_1^+(+1)$	$E_1^-(-1)$	$E_2^+(+2)$	$E_2^-(-2)$	$E'_2^-(+3)$	$E'_2^+(-3)$
$E_1^+(+1)$	$\zeta k + 2(k-1)\mu_B B_\parallel$		$+\sqrt{2}\mu_B B_\perp$			$-\delta$
$E_1^-(-1)$		$\zeta k - 2(k-1)\mu_B B_\parallel$		$+\sqrt{2}\mu_B B_\perp$	$-\delta$	
$E_2^+(+2)$	$+\sqrt{2}\mu_B B_\perp$		$+2k\mu_B B_\parallel$	$+\delta$	$-\sqrt{2}\mu_B B_\perp$	
$E_2^-(-2)$		$+\sqrt{2}\mu_B B_\perp$	$+\delta$	$-2k\mu_B B_\parallel$		$-\sqrt{2}\mu_B B_\perp$
$E'_2^-(+3)$		$-\delta$	$-\sqrt{2}\mu_B B_\perp$		$-\zeta k + 2(k+1)\mu_B B_\parallel$	
$E'_2^+(-3)$	$-\delta$			$-\sqrt{2}\mu_B B_\perp$		$-\zeta k - 2(k+1)\mu_B B_\parallel$

Chart II

	$E_{3/2}^+(+^3/_2)$	$E_{3/2}^-(-^3/_2)$	$E_{5/2}^+(+^5/_2)$	$E_{5/2}^-(-^5/_2)$
$E_{3/2}^+(+^3/_2)$	$k\zeta + (2k-1)\mu_B B_\parallel$		$\mu_B B_\perp$	δ
$E_{3/2}^-(-^3/_2)$		$k\zeta - (2k-1)\mu_B B_\parallel$	δ	$\mu_B B_\perp$
$E_{5/2}^+(+^5/_2)$	$\mu_B B_\perp$	δ	$-k\zeta + (2k+1)\mu_B B_\parallel$	
$E_{5/2}^-(-^5/_2)$	δ	$\mu_B B_\perp$		$-k\zeta - (2k+1)\mu_B B_\parallel$

and $Cp_2{}^*Re$) have been analyzed in terms of a model first proposed by Maki and Berry[16] and elaborated by Rowe and McCaffery (RMcC).[17] Both models take as their starting point the energy level scheme described in the introduction. The excited configurations considered are also expressed in terms of these five MOs. We now proceed to a full description of each model.

d^4 Model.[15] Our earlier work[3,5] showed that the ground configuration for the d^4 metallocenes is $(e_2)^3(a_1)^1$, which gives rise to $^3E_2$ and $^1E_2$ orbital state functions.[2] Of these, the former, together with e_1 or a_2 spin functions, gives rise to one E_1 and two E_2 spin–orbit states. When the methods described by Griffith[18] are used, the states that result from the coupling of these orbital and spin wave functions may be written (Figure 2)

$$E_1^+(\Omega = +1) = -i|-\bar{2}+2+\bar{2}\ \bar{0}\rangle$$

$$E_1^-(\Omega = -1) = +i|-2-\bar{2}+2\ 0\rangle$$

$$E_2^+(\Omega = +2) = -(i/\sqrt{2})(|-\bar{2}+2+\bar{2}\ 0\rangle + |-2+2+\bar{2}\ \bar{0}\rangle)$$

$$E_2^-(\Omega = -2) = +(i/\sqrt{2})(|-2-\bar{2}+2\ \bar{0}\rangle + |-2-\bar{2}+\bar{2}\ 0\rangle)$$

$$E'_2{}^-(\Omega = +3) = +i|-2+2+\bar{2}\ 0\rangle$$

$$E'_2{}^+(\Omega = -3) = -i|-2-\bar{2}+\bar{2}\ \bar{0}\rangle$$

where ±2 represent the e_2 MOs and 0 the a_1 MO. Previously, we showed that for both Cp_2Mo and Cp_2W the MCD spectra were consistent with a E_2 spin–orbit ground state derived from the $^3E_2$ term.[6] With these states as a basis, it is quite straightforward to deduce the matrix elements of the operator

$$\mathcal{H} = \mathcal{H}_{so} + \mathcal{H}_z + \mathcal{H}_d \ldots \qquad (5)$$

where $\mathcal{H}_{so}$, $\mathcal{H}_z$, and $\mathcal{H}_d$ are the Hamiltonians for spin–orbit coupling, the Zeeman effect, and a putative lower symmetry perturbation.[15,17] The energy matrix takes the form (Ω values in parentheses) in Chart I. Here, ζ is the metal d-electron spin–orbit coupling constant, k, the orbital reduction factor, μ_B, the Bohr magneton, and δ, the off-diagonal matrix element due to the low symmetry field.[17] $B_\parallel$ and $B_\perp$ are the parallel (z) and perpendicular (x, y) components of the applied magnetic field, respectively. This matrix introduces spin–orbit coupling in the diagonal elements and mixes the E_1 states through the off-diagonal elements containing δ and $B_\perp$. Ammeter,[19] in an analysis of the EPR spectra of orbitally degenerate metallocenes, has suggested the use of two independent quenching factors. However, as will become clear when we discuss our results, the MCD saturation behavior of our models is not sufficiently sensitive to the value of the spin–orbit coupling parameter to warrant such refinement.

The calculated magnetic properties of the ground state of a d^4 metallocene depend upon the energies and wave functions that result when the above matrix is diagonalized with suitable values for the parameters ζ, k, and δ. In our experiments, these properties are probed via the magnetic circular dichroism of observed electronic spectral bands and, apart from special cases,[20] the saturation behavior of the MCD depends upon both the ground- and excited-state structures.[7] We must therefore consider the nature of the excited states of a d^4 metallocene. In our earlier work on these molecules[6] we showed that the positive C-terms observed are consistent with the assignment to an E_2 excited state arising from the configuration $(e_1)^3(e_2)^4(a_1)^1$. In the present work we find that the experimental magnetization curves for Cp_2Mo and Cp_2W are well fitted using the ground-state model described above and Δa values calculated for the $E_2 \leftarrow E'_2$ transition.

d^5 Model.[16,17] Following RMcC,[17] the d^5 ground configuration is $(e_1)^4(a_1)^2(e_2)^3$, giving states that may be formulated by the double-group representation:[17]

$$\left.\begin{aligned} E_{3/2}^+(\Omega = +^3/_2) &= |-\bar{2}+2+\bar{2}\rangle \\ E_{3/2}^-(\Omega = -^3/_2) &= |-2-\bar{2}+2\rangle \end{aligned}\right\} \quad E_{3/2}\ (=E''; \text{RMcC})$$

$$\left.\begin{aligned} E_{5/2}^+(\Omega = +^5/_2) &= |-2+2+\bar{2}\rangle \\ E_{5/2}^-(\Omega = -^5/_2) &= |-2-\bar{2}+\bar{2}\rangle \end{aligned}\right\} \quad E_{5/2}\ (=E'''; \text{RMcC})$$

With perfect D_5 symmetry, the $E_{5/2}$ component forms the ground state, but under the Hamiltonian (eq 5), the two states mix together and we obtain the following ground-state energy matrix (notation as above; Chart II). This is RMcC's "model 2" of the ground state of the isoelectronic $[Cp_2Fe]^+$.

We have shown previously, using RMcC's model 1, that the excited state must be $E_{3/2}$, arising from the configuration $(e_1)^3(a_1)^2(e_2)^4$. This agrees with the positive C-terms, which we observe for both our rhenocenes. Under model 2, however, the mixing induced by the low-symmetry perturbation makes transitions to $E_{1/2}$ allowed also. These additional excitations are associated with a negative C-term, but since the $^2E_1$ is basically a pure ligand state (the hole is in an orbital that is localized on the ligand), spin–orbit coupling is small, and we do not expect to resolve the separate transitions to $E_{1/2}$ and $E_{3/2}$. We are therefore concerned with the total C-term, which remains positive.

To calculate Δa for any particular choice of parameters, we use the equations of SMK already discussed.[7] For the integration over the angle θ between the applied magnetic field and the molecular axis, we use 10-point numerical quadrature with

(15) Krieger, R.; Voitländer, J. *Z. Naturforsch., A: Phys., Phys. Chem., Kosmophys.* **1972**, *27a*, 1082.
(16) Maki, A. H.; Berry, R. J. *J. Am. Chem. Soc.* **1965**, *87*, 4437.
(17) Rowe, M. D.; McCaffery, A. J. *J. Chem. Phys.* **1973**, *59*, 3786. Herzberg, G. *Molecular Spectra and Molecular Structure III. Electronic Spectra and Electronic Structure of Polyatomic Molecules*; Van Nostrand: Princeton, NJ, 1966.
(18) Griffith, J. S. *The Irreducible Tensor Method for Molecular Symmetry Groups*; Prentice-Hall: Englewood Cliffs, NJ, 1962.
(19) Ammeter, J. H. *J. Magn. Reson.* **1978**, *30*, 299.
(20) Graham, R. G. *Chem. Phys. Lett.* **1987**, *133*, 193.

Gauss–Legendre points and weights. No integration over the other Euler angle is required since there are no nonzero matrix elements of m_z in the particular orbital basis that we are using. Thus, our procedure for simulating a magnetization curve is as follows. For a selection of the parameters δ, k, δ, T, and B, the energy matrix is set up and diagonalized and the value of Δa for all transitions $A \rightarrow J$ calculated from eq 2, which reduces to

$$\Delta a = \cos\theta \{|\langle A'|m_-|J\rangle|^2 - |\langle A'|m_+|J\rangle|^2\}$$

since $\langle A'|m_z|J\rangle = 0$. The resulting Δa is convoluted with the population factors (eq 1), the process is repeated for the 10 values of $\cos\theta$, and the results are multiplied by the appropriate weights and added (eq 3) to give the final $\langle \Delta\epsilon\rangle_0$ for each transition for that particular value of the magnetic field. The whole process is then repeated for further values of B between 0 and 8 T and the resulting theoretical magnetization curve normalized to 100 at its maximum. The theoretical curve is evaluated at about 30 values of B/T chosen from the 200–300 experimental points and the mean-square deviation between the experimental and theoretical points evaluated. The adjustable parameters of the ground-state model are then varied so as to reduce the sum of the mean-square deviations to a minimum by a process of trial and error. Further details concerning this aspect of the curve-fitting process will be described in the following section of the paper where the values of the parameters determined are discussed.

Finally, the values of $g_\parallel$ and $g_\perp$ corresponding to a particular set of parameters are found by diagonalizing the energy matrix to give the splitting, ΔE, of the lowest Kramers doublet at $B_\parallel$ = 5.0 T and $B_\perp$ = 0.0 T, and vice versa. Then, $G = \Delta E/0.46693B$.

Discussion

The MCD method has provided us with excellent optical data for the magnetization of unstable metallocenes. Both methods of analysis succeed in simulating the curves with remarkably little error (Table I). Apart from the root-mean-square error, we have found no statistical criteria for the reliability of our resulting g values, but the error bars given in the table provide useful comparisons between the compounds. We consider first the analysis by method I. The results can be tested by comparison with the EPR determinations of g values for $(tol)_2V$ and Cp^*_2Re. In the case of $(tol)_2V$ the MCD value of 1.94 is in excellent agreement with the EPR value of g_{iso} of 1.99, while for Cp^*_2Re our MCD result of 5.07 is remarkably close to the EPR value of 5.08.[9] However, we must recognize that the EPR result for Cp^*_2Re was determined in a frozen toluene solution where the distortion that allows $g_\perp$ to depart from zero may well be very different from that in an argon matrix.[19]

When we move to method II (right-hand side of the table), the fitting of our data to detailed quantum mechanical ground-state models is seen to give results that are very close to those obtained with the SMK axial model. The superimposition of magnetization curves measured at different temperatures for Cp_2W, Cp_2Re, and Cp^*_2Re shows that there are no low-lying electronic energy states which can be significantly populated at the higher temperatures and that there is no detectable mixing of electronic states by the magnetic field. The appearance of nesting curves for Cp_2Mo indicates that mixing may be significant. Magnetization curves measured on this molecule at the same temperatures and at four different wavelengths showed the same nesting behavior. This suggested to us that the origin of the nesting might lie in the ground state of the molecule and, as the d^4 energy matrix shows, if ζ and/or k are sufficiently small, there is a possibility of mixing of states by the magnetic field and of population of states other than the lowest Kramers doublet. Effects of this type should be reproduced by the d^4 model described above and, accordingly, we attempted to fit the nested molybdenocene data directly without first removing the B-term. As might have been anticipated, the best fits were obtained with very small values of the product δk, but no really satisfying fit of the data could be obtained, the rms deviation being of the order of 5.5. When the B-term-corrected data were used, much better fits were obtained (table), and we therefore conclude, contrary to our earlier hypothesis, that the origin of the nesting lies primarily with B-term mixing in the excited states. However, we recognize that, by subtracting out a B-term contribution from the raw data, we may have removed a small ground-state effect upon the magnetization curve, which our model would, in principle, reproduce. The absence of this corrected component in the modified data may be the reason for the fact that the molybdenocene data give one of the two poorest fits among the five molecules examined.

For the d^4 molecules the energy matrix shows that, in the absence of the low-symmetry field represented by δ, any realistic value of the spin–orbit coupling parameter splits out a Kramers doublet with a $g_\parallel$ value (per electron) of $2(k + 1)$. Values of k less than 1 and large δ values bring $g_\parallel$ into the range expected from the previous fits to eq 4. There appears to be no way of separating these effects, and we have therefore taken fixed values of ζ[6,21] and found pairs of values of k and δ that give the best fit to the experimental data. The figures in the table show that good fits of the experimental data can be obtained for values of k down to 0.6 and 0.4 for Cp_2W and Cp_2Mo, respectively. These figures set a lower limit for k. In all cases $g_\perp$ is found to be very small. The small $g_\perp$ values ($\leq$0.1) offer an explanation as to why incorporation of this parameter into method I produced no improvement of the fit.

In principle, the same interdependence of ζ, δ, and k should be observed in the d^5 model, although there are slight differences. In the case of the rhenocenes, however, we find that, for all k and ζ parameter combinations giving a good fit, nonzero values of δ always reduce the quality of the fit. This being so, a choice of ζ leads to a value of k with $g_\perp$ rigorously zero. We choose ζ = 1800 cm^{-1} in view of a recent analysis of the photoelectron spectrum of Cp^*_2Re.[9] Since an EPR signal has been observed for a frozen toluene solution of decamethylrhenocene at 10 K, $g_\perp$ cannot be exactly zero,[12,14] but the EPR evidence does place its value below 0.34. Again, we must be aware of the possible differences imposed upon the molecule by the two different media.[19]

In their treatment of $[Cp_2Fe]^+$, RMcC considered the addition to their model of a mixing of the $^2A_{1g}$ state into the ground state, "model 3". We also investigated this addition to the ground-state model for the d^5 systems, but we found the fit of theoretical to experimental magnetization curves was very insensitive to this addition to the model, being neither significantly improved nor diminished by it. We conclude, therefore, that our data do not permit us to make any definitive statement concerning this possible mixing of states.

Conclusions

The measurement of optical magnetization curves via MCD has enabled us to determine $g_\parallel$ for unstable metallocenes. Where comparisons are possible, the results agree well with more precise EPR determinations.

In earlier work, we used measurement of $\Delta A/A$ to determine $g_\parallel$ values for these metallocenes.[6] The present results show that these measurements were subject to substantial errors. We consider that, even with great care, the measurement of $\Delta A/A$ is subject to greater uncertainties than the MCD magnetization method.

The d^4 metallocenes, Cp_2W and Cp_2Mo, have two unpaired electrons and an E_2 ground spin–orbit term. In a magnetic field, this term is split by $2g_\parallel\mu_B B$ ($6.14\mu_B B$ and $5.5\mu_B B$ for Cp_2W and Cp_2Mo, respectively). The degree of delocalization cannot be determined at present without assumptions concerning the values of spin–orbit coupling constant and low-symmetry distortion parameters. The value of $g_\perp$ is found to be $\leq$0.04.

The d^5 metallocenes, Cp_2Re and Cp^*_2Re, have one unpaired electron in an e_2 orbital, giving rise to an $E_{5/2}$ ground spin–orbit term. The measurements show that this term is split by $5.30\mu_B B$ and $5.08\mu_B B$ for Cp_2Re and Cp^*_2Re, respectively, in the magnetic field. As expected, the degree of delocalization onto the ligands

(21) Griffith, J. S. *The Theory of the Transition-Metal Ions*; Cambridge University: Cambridge, England, 1961.

is greater for the methylated derivative. Our analysis indicates that any low-symmetry distortion is much smaller than for the d^4 metallocenes.

Acknowledgment. We thank the United Kingdom Science and Engineering Research Council and the Royal Society for their support of this work.

Registry No. Cp_2Mo, 51370-80-0; Cp_2W, 51481-44-8; Cp_2Re, 56261-86-0; Cp_2^*Re, 98814-97-2; $(tol)_2V$, 12131-27-0.

Stacked Complexes of Iridium and a Novel Form of Charge Compensation

Paul G. Rasmussen,* J. Bruce Kolowich, and Juan Carlos Bayón†

Contribution from the Department of Chemistry, University of Michigan, Ann Arbor, Michigan 48109. *Received November 18, 1987*

Abstract: Mixed valence metal chain compounds based on the monoanion $[Ir(CO)_2Tcbiim]^-$ were investigated (Tcbiim = 4,4′,5,5′-tetracyano-2,2′-biimidazole, a dianion). These compounds were prepared by inert atmosphere electrochemical oxidation with a variety of alkyl ammonium cation based electrolytes. Synthetic details are presented for the preparation of several asymmetric alkyl ammonium cations, and the subsequent electrolyte salt preparation. The technique for electrochemical oxidation is described in detail. Single-crystal X-ray solutions are presented for three complex Ir(I) salts: $NEt_3Me[Ir(CO)_2Tcbiim]\cdot{}^1/_2CH_3CN$, $NEt_2Me_2[Ir(CO)_2Tcbiim]$, and a dication salt $NEt_2Me(CH_2)_4NEt_2Me[Ir(CO)_2Tcbiim]_2$. The first of these crystallizes in the space group *Pnnm* with $a = 6.918$ Å, $b = 22.223$ Å, $c = 15.101$ Å, and $Z = 4$. A final agreement of $R = 4.25\%$ for 133 parameters with 972 retained data was obtained. The second crystallized in the space group $P2_12_12$ with $a = 7.074$ Å, $b = 19.698$ Å, $c = 15.336$ Å, and $Z = 4$. The obtained final agreement was $R = 3.94\%$ for 236 parameters with 1505 retained data. The dication structure was refined in the nonstandard space group $P22_12_1$ with $a = 15.751$ Å, $b = 7.233$ Å, $c = 19.135$ Å, and $Z = 4$. A final agreement of $R = 5.1\%$ for 130 parameters with 789 retained data was found. Solid-state packing for this series of compounds is discussed. Packing diagrams reveal molecular interactions responsible for earlier observations of thermochromic behavior. A series of insoluble mixed valence compounds formulated as $[cat]_5[Ir(CO)_2Tcbiim]_6[an]$ where [cat][an] denotes included supporting electrolyte were prepared. Conductivity data are presented. A reaction of $[cat]_4[Ir(CO)_2Tcbiim]_6$ with an isoelectronic analogue of the stacking unit $[Pt(CN)_2Tcbiim]^{2-}$ produced a unique one-dimensional alloy in single-crystal form. This compound, $[NEt_3Me]_3[Ir(CO)_2Tcbiim]_2[Pt(CN)_2Tcbiim]\cdot 3CH_3CN$, crystallized in the space group $P2_1$ with $a = 13.412$ Å, $b = 6.874$ Å $c = 13.409$ Å, and $\beta = 111.21°$. Here, $Z = 2$, however; since there is one metal atom in the asymmetric unit, the stacking units are disordered along the stack. Perspective plots clearly reveal a metal atom chain. Final agreement of $R = 4.01\%$ was observed for 223 parameters with 2227 retained data.

In the realm of class III mixed-valence compounds, there are relatively few that have been synthesized by conscious design, and none that we are aware of wherein a hetero bimetallic system yields a crystallographically identical site for two metals in different oxidation states. We report here on the synthesis and characterization of such a system based on complexes of tetracyanobiimidazole. Some of the coordinating tendencies of this ligand have been previously reviewed.[1]

The starting point for this system is the planar anion $[Ir(CO)_2Tcbiim]^-$ where $H_2Tcbiim$ is 4,4′,5,5′-tetracyano-2,2′-biimidazole, an acidic molecular comparable to oxalic acid. This planar ion associates weakly in solution and precipitates as a brightly colored solid. The color of the solid varies with the counter cation. Under electrolytic oxidation this ion associates strongly and forms a linear-chain mixed-valence semiconductor that grows on the anode. This material has an unusual charge compensation mode. Partial oxidation of the iridium apparently leads to disorder on the counter cation site. To solve this problem we introduce the isoelectronic ion $[Pt(CN)_2Tcbiim]^{2-}$ into the solution. The structure and properties of the pure linear chain and the novel one-dimensional alloy are described below.

The isolation of single crystals of iridium chain compounds has proven difficult, although classic work by Ginsberg et al.[2] and Reis[3] showed that it could be done. The isoelectronic substitution method we describe may prove generally useful in aiding crystallization in partially oxidized systems.

Experimental Section

Physical Measurements. Elemental analyses were performed by Spang Microanalytical Laboratory, Eagle Harbor, MI 49951, or Galbraith Laboratories Inc., Knoxville, TN 37921.

Infrared spectra (4000–200 cm^{-1}) of samples confined as KBr pellets, or as Nujol mulls placed between NaCl, KBr, or AgCl plates, were recorded on a Perkin-Elmer Model 1330 grating spectrophotometer.

Proton NMR spectra were recorded on a Brucker WM-360. All proton resonances are reported relative to TMS, except those recorded in D_2O, which are reported relative to DSS.

Two contact pellet conductivities were measured with a simple press. The base of the press was constructed from a solid block of aluminum and the barrel and plunger are composed of steel. The plunger is insulated from the barrel with a nylon sleeve, and conductivity is measured from the plunger to the base while pressure is applied.

Scanning electron microscope work was performed on a Hitachi Model S-570. The geology department of the University of Michigan acknowledges support from NSF Grant No. BSR-83-14092 for the purchase of this new microscope in 1985.

Electron microprobe analysis was performed on a Cameca-MBX, purchased for the University geology department with support from NSF Grant No. BAR-82-12764 in 1984.

Powder diffraction patterns were recorded on a North American Phillips Co. type 52056-8 Debye-Sherrer camera, mounted on a Phillips X-ray source equipped with a Copper Kα X-ray tube.

† Present address: Universitat Autônoma de Barcelona, Bellaterra, 08193 Barcelona, Spain

(1) Avery, J., Dahl, J. P., Ed. *Understanding Molecular Properties*; D. Reidel: Hollard, 1987; pp 187–194.
(2) Ginsberg, A. P.; Koepke, J. W.; Hauser, J. J.; West, K. W.; DiSalvo, F. J.; Sprinkle, C. R.; Cohen, R. L. *Inorg. Chem.* **1976**, *15*, 514.
(3) Reis, A. H.; Peterson, S. W. *Ann. N.Y. Acad. Sci.* **1978**, *313*, 560.

0002-7863/88/1510-7042$01.50/0